ACADEMIC PRESS

Available online at www.sciencedirect.com
SCIENCE DIRECT®

Journal of Catalysis 214 (2003) 53–67

JOURNAL OF CATALYSIS

www.elsevier.com/locate/jcat

Carbon-supported palladium catalysts. Molecular orbital study

Irena Efremenko * and Moshe Sheintuch

Department of Chemical Engineering, Technion–Israel Institute of Technology, Haifa, Israel 32000

Received 20 May 2002; revised 16 October 2002; accepted 7 November 2002

Abstract

Geometric and electronic structures of palladium clusters supported on activated carbon (Pd_n/AC) are analyzed using semiempirical quantum chemical modeling for $n = 1$–22. Qualitative reliability of the results is checked by DFT calculations for $n = 1$–6. Supported Pd atoms and clusters are shown to be strongly bound to unsaturated and defect surface sites. In such positions, interaction of Pd atoms with the support is much stronger than that with each other. That provides the driving force for atomic dispersity of Pd/AC catalysts. Geometry of small clusters is determined by morphology of an adhesion position. Nanosized particles form compact three-dimensional structures with close-packed triangular surfaces. AC support causes notable excitations in the electronic structure of metal atoms directly bound to the support, resulting in the direct nucleation of *fcc*-like structures. These excitations are quickly extinguishing when moving far from the support surface.

Keywords: Supported catalysts; Clusters; Palladium; Activated carbon; Semiempirical quantum chemical modeling; DFT

1. Introduction

Supported catalysts are typically made of transition metal clusters with diameters less than 5 nm anchored to the support surface. They experience strong influence of the support, which has major implications on catalyst stability and reactivity. This paper is devoted to the study of Pd catalysts interactions with activated carbon (AC). Nanosized particles show unique physical and chemical properties [1–4]. As a rule, small transition metal clusters are characterized by unusual symmetries and contracted interatomic distances as compared to those of the bulk [5], by loss of metal properties [6] and by atypical magnetic behavior [7]. However, available data on bare clusters have given only minor contribution to our understanding of the structure and properties of supported catalysts since interaction with the support influences the morphology and electronic structure of metal particles [8]. Numerous fundamental investigations on the morphology, nature, and reactivity of supported catalysts led to impressive progress in understanding their chemistry at the atomic level (for recent reviews, see, e.g., [9–14]). Yet such questions as bulk and surface structure of nanosized supported particles, cluster size distribution, and its relationship to the atomically dispersed metal phase and metal-induced changes in the support surface remain open. Because of the extremely small size of supported particles, experimental identification of these characteristics is a very difficult task [9,11].

At this point quantum chemical calculations can be of large value. Modern density functional theory (DFT) calculations are the methods of choice for such studies; however, these methods are still computationally demanding for treatment of a large transition metal system. The lack of accurate experimental information about the structural aspects of the catalyst–support interface presents another serious problem in the theoretical modeling of supported catalysts. Thus, a high-level quantum chemical study of the structure and reactivity of supported transition metal clusters is still at its early stage [15,16]. DFT methods were applied for investigation of adhesion of the metal atoms and up to six-atomic clusters of Pd [17–25], Pt [26], Cu [22,23,25,27,28], Ag [21,22,27], Au [27], Ni [22,23,29,30], and Co [30] on TiO_2 and MgO. Other supports (SiO_2, Al_2O_3) attracted significantly less attention [31–36]. To the best of our knowledge, no published theoretical results are available on the transition metal clusters supported on activated carbon (AC). Probably, this is due to its extremely complex surface chemistry.

* Corresponding author.
E-mail address: chrirena@techunix.technion.ac.il (I. Efremenko).

0021-9517/03/$ – see front matter
doi:10.1016/S0021-9517(02)00103-3

Activated carbon supports consist generally from small graphite crystallites with highly disordered, irregular, rough and heterogeneous surface. The "zigzag" configuration of edges of carbon layers is the most common in a wet environment [37,38]. Pretreatment of activated carbons causes reorganization of their porous [39] and surface structures [40–42] and influences significantly the adsorptive and chemical properties of the support [43]. Depending on the AC nature, pretreatment, and application history, a multitude of surface functional groups and surface ensembles are formed, so the determination of local AC surface structure and, specifically, of the active sites for anchoring of supported transition metal particles is not straightforward. Therefore, in spite of the wide application of Pd/AC catalysts and numerous publications devoted to their performance in catalytic processes, the fundamental studies of these catalysts are rather scarce [44,45].

This work presents the results of semiempirical EH (and some DFT) modeling of adsorption and growth of $Pd_{1–22}$ particles in surface sites of activated carbon with various geometric and chemical natures modeled by relatively large $C_{35}H_{11}$–$C_{65}H_{25}$ clusters. The following problems are addressed:

1. Relative stabilities of the regular zigzag and several defect surface positions for capping of a Pd atom and their coverage dependence;
2. Influence of the saturation of surface C-atoms and of the nature of surface groups (i.e., AC pretreatment) on the Pd–AC interactions;
3. Relationship between the atomically dispersed metal phase and agglomeration;
4. Geometric and electronic structures of very small palladium particles supported in different coordination positions on AC surface;
5. Support-induced directions for the growth of nanosized palladium particles.

The main attention is paid to the support-induced changes in the electronic structure of the metal particles and to the geometric structure of relatively large Pd_n/AC ($n > 10$) clusters with an average size of about 1 nm. Presently, such clusters are the most difficult for investigation since they are too small for experimental observation and too large for modeling by high-level theoretical methods. The obtained results are compared with the corresponding experimental and theoretical data on the supported and bare clusters and on bulk palladium surfaces.

Between validity of computational model and level of theoretical approach, the former issue seems to be more important for poorly investigated systems. The initial approach to such systems should provide a qualitative understanding of the most important features and basis for following quantitative calculations. Literature analysis [46,47] and our own experience [48,49] show that extended Hückel (EH) based methods remain the best semiempirical tool for handling large transition metal systems. Such methods are known to provide trustworthy qualitative trends and electronic structures from the molecular orbital point of view [50] but neither absolute energetic values nor optimized bond distances calculated by EH-based methods are reliable themselves. The computational approach applied here was also used for modeling of bare palladium clusters [48] and ions [49]. Later, DFT calculations [51] confirmed the obtained qualitative trends. Comparison of the binding energies computed for Pd_n clusters and ions with both methods shows simple linear relationships between the two (Fig. 1). We feel that this justifies the use of EH methods for predicting qualitative trends in large Pd_n/AC systems. Besides, qualitative credibility of the present results is validated by DFT calculations of $Pd_{1–6}$ interactions with small $C_{10}H_6$ cluster, modeling the simplest adsorption site on the AC surface. The detailed DFT results will be presented elsewhere. We compare here the two methods and show a simple linear relation between their predictions. For large palladium clusters, the EH energetic values can be corrected to estimate DFT values.

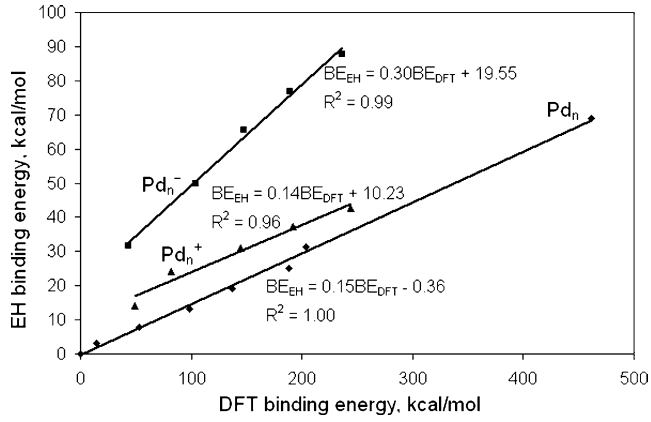

Fig. 1. Relationship between binding energies obtained by DFT and EH methods for the Pd_n ($n = 2–13$), Pd_n^+, and Pd_n^- ($n = 2–6$) clusters.

The remainder of the paper is organized as follows. Computational methods and models are described in the next section. In Sections 3 and 4, the computational data on atomic palladium adsorption and cluster growth in different coordination positions on an AC surface are presented. Implication of the obtained results into the understanding of the Pd–AC interactions is discussed in Section 5. Section 6 gives our conclusions.

2. Computational methods and models

Semiempirical calculations are performed using the extended Hückel technique [52] modified by the core–core repulsion term. The method is essentially similar to the ASED MO (atom superposition and electron delocalization molecular orbital) approach [53]. The differences are that (i) as in the "classical" extended Hückel theory, the unmodified "weighted" Wolfsberg–Helmholz formula with the distance-independent Hückel constant $K = 1.75$ [54],

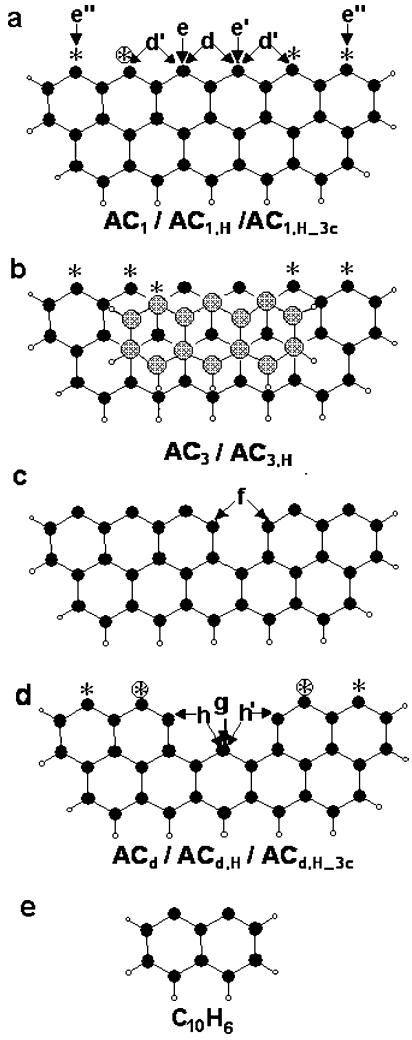

Fig. 2. Model clusters used for representation of active adsorption sites on the surface of activated carbon. In the notations, AC_1, AC_3, and AC_d stand for the unsaturated clusters modeling the regular one- and three-layer zigzag edges and the defect site on the AC surface, respectively; $AC_{1,H}$, $AC_{3,H}$, and $AC_{d,H}$ stand for the same clusters in which the marked carbon atoms are saturated with hydrogen; in the AC_{1,H_3c} and AC_{d,H_3c} clusters the hydrogen atoms are removed from the circle-star marked positions.

(ii) the standard Hückel parameters [55], and (iii) the repulsive term as formulated by Calzaferri et al. [56] are employed in the applied scheme. DFT calculations have been carried out using Gaussian98 package [57] at the B3LYP level of theory [58,59]. The relativistic effective core potential basis set of double-ζ quality LANL2DZ was employed for Pd [60] and C [61] atoms; H atoms were described in the cc-pVDZ basis set [62]. Both EH and DFT calculations were performed for the lowest multiplet state.

To represent structural irregularities holding dangling bonds as well as the regular basal graphite plane, in the EH calculations, the surface of activated carbon was modeled by the one-layer $C_{37}H_{11}$ (AC_1) and three-layer $C_{65}H_{25}$ (AC_3) clusters (Figs. 2a and 2b). Surface defects were obtained by removing carbon atoms from the AC_1 model cluster (Figs. 2c and 2d). The clusters were assumed to keep a fixed graphite structure with nearest neighboring C–C bond lengths of 1.42 Å and interlayer distances of 3.35 Å. Saturation of dangling bonds on the AC surface was achieved by termination of the carbon atoms marked with stars by H atoms or by OH groups with C–H, C–O, and O–H bond lengths of 1.0, 1.43, and 1.0 Å, respectively. The H-terminated clusters from Figs. 2a, 2b and 2d are noted as $AC_{1,H}$, $AC_{3,H}$, and $AC_{d,H}$, respectively. In the DFT calculations a small $C_{10}H_6$ cluster (Fig. 2e) modeling the zigzag edge on the AC surface with full geometry optimization was applied. For comparison purposes, the same cluster with the frozen geometry was used in several parallel EH calculations.

The Pd_n–AC binding energy (BE) is determined as

$$\mathrm{BE} = E(\mathrm{Sup}) + n \times E(\mathrm{Pd}) - E(\mathrm{Pd}_n/\mathrm{Sup}), \quad (1)$$

where $E(\mathrm{Pd}_n/\mathrm{Sup})$, $E(\mathrm{Sup})$, and $E(\mathrm{Pd})$ are the energies of the adsorptive complex, the corresponding model cluster, and a Pd atom, respectively. In several calculations, one H atom of a $AC_{1,H}$ model cluster and two H-atoms of a $AC_{d,H}$ cluster were removed. The resulting clusters are noted as AC_{1,H_3c} and AC_{d,H_3c}, respectively. In these cases, the binding energy was calculated as

$$\mathrm{BE}_1 = (\mathrm{Sup}) + n \times E(\mathrm{Pd}) - E(\mathrm{Pd}_n/\mathrm{Sup}) - (m/2) \times E(\mathrm{H}_2), \quad (2)$$

where $E(\mathrm{Sup})$ corresponds to the H-terminated $AC_{1,H}$ or $AC_{d,H}$ model clusters, m is the number of the removed H atoms, and $E(\mathrm{H}_2) = -33.771$ eV is the energy of a hydrogen molecule calculated by the same method.

3. Atomic palladium adsorption on the AC surface

As a first step, we consider the relative stabilities of different coordination positions on the regular and defect sites of the AC surface toward trapping of a single palladium atom and the nature of the Pd–AC interactions at various coverages. Fig. 3 shows schematically several calculated structures of atomic Pd adsorption, the corresponding binding energies, and the optimized shortest Pd–C bond distances.

3.1. Adsorption of a single palladium atom on the AC surface

Adsorption centers on the carbon atoms with dangling bonds, especially on the *g* and *h* defect sites, cap Pd atoms with high exothermic effect. The basal plane of the AC support (Fig. 3a, *a*–*c* positions) demonstrates very low ability to trap Pd atoms and clusters. The large energy difference between *d* position, which is the most stable on the regular zigzag edge, and the nearest *a*–*c*, *e* sites indicates high activation barrier for surface diffusion of an adsorbed palladium atom. The interlayer insertion of a Pd atom (not shown in the figure) is endothermic for all possible positions.

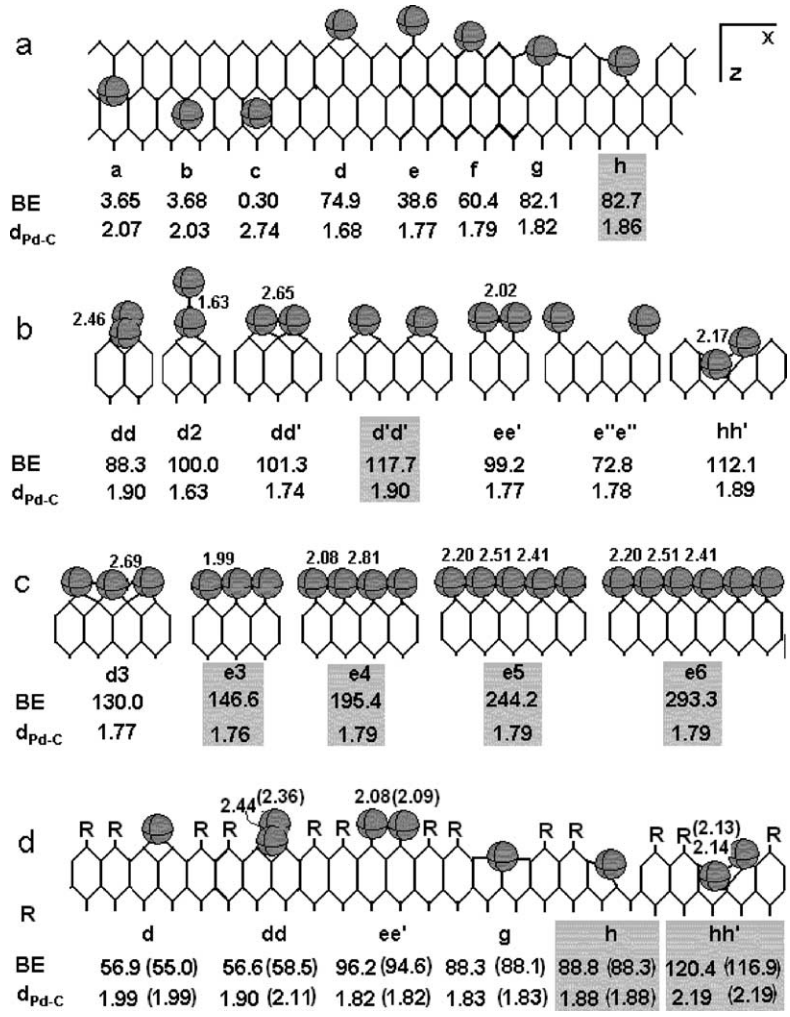

Fig. 3. Atomic palladium adsorption in different surface positions of activated carbon, corresponding binding energies (BE, kcal/mol), and optimized shortest Pd–C distances (Å) for (a) single Pd atom, (b) two-atom cluster and (c) increasing coverage on an unsaturated surface, and (d) single Pd atom and Pd_2 clusters on saturated surfaces. At each "coverage," values corresponding to the most stable arrangement are shadowed. For the saturated model clusters, the first values correspond to R = H and values in parentheses correspond to R = OH.

Two main kinds of interaction between carbon and palladium atoms are evident from the Mulliken population analysis (Table 1). The first one has obviously a donor–acceptor nature: with respect to the stable $4d^{10}5s^{0}5p^{0}$ configuration, the Pd $5s$ orbital accepts significant electron density from the nearest C atoms and Pd $4d$ orbitals donate a large electron density in the opposite direction. This latter part of electron density is distributed between surface carbon atoms not involved in the bonding with palladium (those marked with stars in Fig. 2a) and contributes to compensation of a deficiency in the aromatic electronic structure of unsaturated rings. The best overlapping between Pd $4d$ orbitals and the π system of the support is achieved in the two-coordinated d site. The electronic structure of the adsorbed palladium atom in this position is extremely excited with notable donation from almost all $4d$ orbitals, resulting in the net Mulliken charge of $+1.32$.[1] The second kind of interaction, providing significantly lower energy gain, occurs for palladium adsorption in the onefold e coordination position. In this case, a considerable charge flow from the support to the adsorbate is accompanied by smaller back-donation, leading to the total charge on the adsorbed Pd atom of -0.41. In this position the Pd atom forms essentially a σ bond with the nearest C atom and almost does not interact with the aromatic π system. These two positions present two limiting cases of Pd–AC interactions. For other locations, the excitations in the atomic orbital occupations of adsorbed Pd atoms are in between and depend largely on the geometric structure and chemical nature of a particular AC coordination

[1] The Mulliken charges have to be analyzed with care due to the known limitations of the method; probably, they correctly represent the charge flow under the formation of related bonds, but not the real atomic charges.

Table 1
Mulliken analysis of the electronic structure of Pd atoms supported in different coordination sites on the AC surface

Position[a]	AC_1, AC_d				$AC_{1,H}$, $AC_{d,H}$			
	5*s*	5*p*	4*d*	σ[b]	5*s*	5*p*	4*d*	σ
d	0.26	0.09	8.33		0.48	0.01	9.24	
*d*2[c]	0.52	0.27	8.11		0.29	0.16	7.90	
	0.77	0.03	9.43	0.68	0	0.02	9.38	0.27
dd	0.28	0.01	9.06		0.17	0.11	8.85	
dd′	0.33	0.04	8.96	0.04				
d′*d*′	0.44	0.02	9.15	0				
e	0.62	0.05	9.75					
ee′	0.52	0.03	9.20	0.32	0.52	0.03	9.29	0.31
h	0.54	0.09	9.37		0.39	0.15	9.12	
hh′	0.47	0.08	9.42	0.20	0.34	0.14	9.11	0.21
*e*6	0.60	0.06	9.45					
	0.56	0.07	9.26	0.25				

[a] AC_1 and AC_d stand here for the model clusters shown in Figs. 1a and 1d, respectively; $AC_{1,H}$ and $AC_{d,H}$ refer to the same clusters with the carbon atoms marked with stars saturated with H atoms; for the notations of surface positions see Fig. 2.

[b] Reduced overlap population between two nearest Pd atoms.

[c] First line corresponds to the Pd atom directly bound to the AC surface.

center. High adsorption energies for the defect *g* and *h* sites are due to the formation of several Pd–C bonds and to the stabilization of the π-electronic system of several nearest neighboring aromatic rings.

3.2. Coverage dependence of palladium adsorption on the AC surface

The above two kinds of Pd–AC interactions show different behavior at increasing concentration of adsorbed Pd atoms (Figs. 3b and 3c). For the primarily donor–acceptor type of interaction, the Pd 4*d* to AC donation notably decreases with simultaneous increase in the back-donation to Pd 5*s* AO's. That causes significant weakness in the metal–AC bonding, even though the metal atoms are not bound to each other (*dd*′ structure). Thus, for such interactions the adsorption is stronger when the adsorbed atoms are placed as far from each other as possible (*d*′*d*′ structure). This is the most stable arrangement of palladium atoms on the regular zigzag edge of the AC surface at low concentration. In contrast, the adsorption becomes much stronger when two palladium atoms occupy nearest onefold positions (*ee*′ case). Correspondingly, donation from the palladium 4*d* orbitals to the support is much more pronounced for this dimer than for the single palladium atom in the *e* position.

Due to the support-induced changes in the Pd electronic structure, the interatomic bond lengths in the supported Pd_2 clusters are shorter than those in the gas-phase dimer (2.53 Å), its anion (2.19 Å), and cation (2.22 Å) calculated by the same method [49]. As was shown earlier [49], both an increase in the 5*s* AO occupation and decrease in the 4*d* electron density induce shortness and strengthening of the Pd–Pd bond. The metal–support interactions in the Pd/AC catalyst provide these two effects simultaneously. As a result, the Pd–Pd bond occupations in supported Pd_2 clusters sitting in the *d*2, *ee*′, and *hh*′ positions are 0.676, 0.322, and 0.204, respectively, in comparison with 0.087 in a free Pd_2 cluster, 0.385 in Pd_2^-, and 0.162 in Pd_2^+. It should be emphasized that in all considered cases the interaction of palladium atoms with the support is by far stronger than Pd–Pd bonding and adsorbent-induced stabilization of the support surface significantly contributes to the resulting binding energy. For this reason, at low loadings, no cluster nucleation takes place; additional metal atoms are expected to occupy available positions on the AC surface.

Additional surface palladium atoms (Fig. 3c) further weaken the twofold *d* positions while for the onefold coordination the binding energy per Pd atom increases and becomes coverage-independent at $n \geqslant 3$. The energetically preferential adsorption sites on the zigzag edges of the AC surface at monolayer coverage are onefold *e* positions with the optimized Pd–C distances of 1.79–1.84 Å and the adsorption energy of 48.9 kcal/mol per metal atom. The Pd atoms in such a chain are not equivalent: atoms, which largely donate their 4*d* electron density, alternate with those showing slightly more pronounced electron reception. That in turn leads to the charge oscillations in the range of ± 0.1 with positively charged atoms forming shorter Pd–C bonds. The Pd–Pd bond lengths in such a chain are 2.5 Å with bond occupation of 0.165. That is significantly higher than the corresponding values for the bulk palladium (0.044) and its gas-phase dimer (0.087) calculated by the same method.

3.3. Functional groups on the AC surface

Saturation of dangling surface bonds (Fig. 3d) suppresses the distant interactions of supported Pd atoms with the aromatic π system. That leads to partial relaxation of the palladium electronic structure and causes weakness of the Pd–AC interactions of the donor–acceptor kind. The weakness is significant ($\sim$25%) for *d* position and is feebly marked for the *ee*′ dimer. A diminutive strengthen of the Pd–AC bonding accompanies partial saturation of surface bonds for the checked defect sites. As a result, the defect sites became much more stable than all considered positions on the zigzag edges. The nature of the surface group (H or OH) has only a minor influence on the palladium adsorption; however, for the most stable adsorption positions the Pd–AC interaction is 1.5–3.5 kcal/mol weaker in the presence of hydroxyl group than in the presence of H atoms. At the same time, the overlap populations between palladium and carbon atoms are slightly larger in the former case. The total decrease of the adsorption energy in the presence of hydroxyl groups is due to the adsorbent-induced suppression of the π interaction between C and O atoms, which is responsible for the charge flow from the aromatic π system to oxygen and presents the important constituent of

efficient C–O bonding. This regularity demonstrates the significant contribution of the palladium-induced changes in the substrate electronic structure on the resulting adsorption energy.

4. Palladium clusters adsorbed on the AC surface

An increase of palladium loading above the monolayer coverage leads to the cluster nucleation. In this section, we discuss the geometric and electronic structures of small (few atomic) and relatively large (∼20 atomic) palladium clusters anchored in various coordination positions on the AC surface. First, we consider two nearest neighboring C atoms on the regular zigzag edge of saturated $AC_{1,H}$ model clusters as the simplest adhesion position. The EH results for $Pd_{1–6}$/AC clusters are compared with those obtained by DFT calculations. To check how the supported particles influence the surface structure of activated carbon, we replaced one of the surface H atoms with palladium and considered the adhesion of growing clusters in the corresponding three-center adsorption position. Finally, the effect of the morphology of adhesion position on the cluster growth is tested on the examples of three-layer model cluster and of the model defect site.

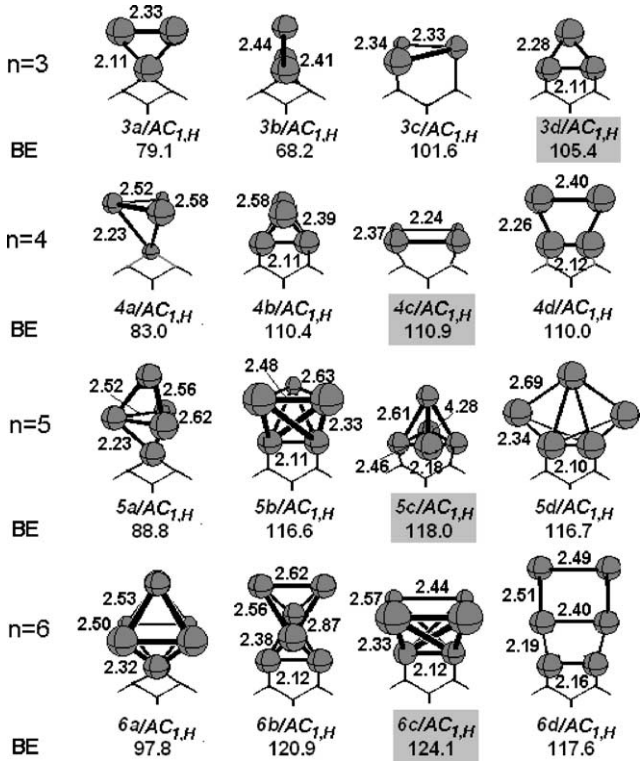

Fig. 4. Optimized structures and corresponding binding energies (BE, kcal/mol) of $Pd_n/AC_{1,H}$ ($n = 3$–6) clusters. For each n, values corresponding to the most stable arrangement are shadowed.

4.1. Pd_n ($n = 3$–6) clusters in the two-center adsorption position (EH and DFT results)

Adhesion of $Pd_{3–6}$ clusters to the two-center coordination site by Pd atoms sitting in the onefold e positions is energetically much more favorable than that by one Pd atom in the twofold d position (Fig. 4). As was shown earlier on the example of small palladium cations [49], involvement of spatially directed 4d electrons into the Pd–Pd bonding favors the formation of planar configurations. Due to the large deficit in the 4d electron density and total positive charge of the first-layer Pd atoms adsorbed in the onefold positions (see Table 2), formation of the planar configurations appears to be the most stable for the Pd_4 and stable enough for the Pd_5 and Pd_6. Excitations in the electronic configuration of palladium atoms quickly extinguish when moving far from the support surface so that even the second-layer Pd atoms have electronic structure very similar to that of the bulk. That results in the elongation of intermetallic bonds with increasing distance from the AC surface and in decreasing binding energy per Pd atom with cluster growth. Nevertheless, for the most stable structures, the

Table 2
Mulliken analysis of the electronic structure and bond population in $Pd_n/AC_{1,H}$ ($n = 3$–6) clusters

Cluster[a]	Layer	5s	5p	4d	σ_{ii}[b]	σ_{ij}[c]
3d	I	0.37	0.13	9.08	0.25	0.11
	II	0.04	0.03	9.74		
4b	I	0.39	0.14	9.00	0.24	0.10
	II	0.08	0.06	9.81	0.06	
4c	I	0.22	0.09	9.42	0.14; 0.18	
4d	I	0.39	0.14	9.08	0.26	0.13
	II	0.05	0.05	9.79	0.11	
5c	I	0.39	0.15	9.00	0.19	0.11; 0.10[d]
	II	0.13	0.06	9.87	0	0.06
	III	0.08	0.05	9.71		
5d	I	0.406	0.16	9.03	0.19	0.11; 0.10[d]
	II	0.058	0.04	9.88	0	0.05
	III	0.072	0.06	9.69		
6c	I	0.41	0.15	8.97	0.26	0.13
	II	0.09	0.07	9.80	0.07; 0.11	
6d	I	0.39	0.14	9.08	0.25	0.14
	II	0.07	0.08	9.72	0.12	0.09
	III	0.05	0.04	9.90	0.09	
$Pd(111)$[e]	Surface	0.11	0.09	9.80	0.05	0.04[f]
$Pd(100)$[e]	Surface	0.10	0.08	9.82	0.05	0.04[f]
$Pd(110)$[e]	Surface	0.09	0.07	9.84	0.05	0.05[f]

[a] See Fig. 4.
[b] Reduced overlap population between two nearest Pd atoms from the same layer.
[c] The same for the given and upper-layer atoms.
[d] The same for the given and third-layer atoms.
[e] Calculated by the same method for the 43-, 46-, and 42-atomic model clusters of the (111), (100), and (110) faces, respectively, with frozen bulk palladium geometry.
[f] Reduced overlap population between surface and second-layer Pd atoms.

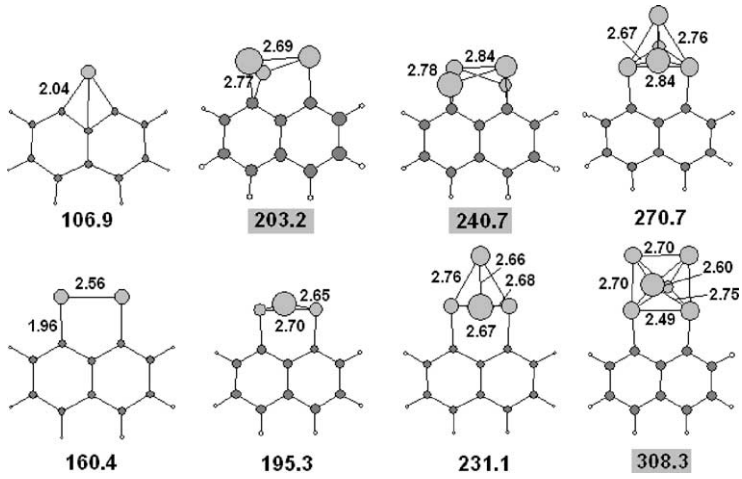

Fig. 5. DFT optimized structures and corresponding binding energies (BE, kcal/mol) of $Pd_n/C_{10}H_6$ ($n = 1$–6) clusters.

interaction energy of the Pd_n–AC bonding, calculated with respect to the stability of the corresponding Pd_n clusters, remains in the range of 97.6–98.9 kcal/mol. Relative stabilities of the planar configurations decrease with increasing cluster size, and for Pd_5 and Pd_6 cluster three-dimensional 5*c* and 6*c* structures become more stable than other isomers.

Fig. 5 presents optimized geometries and corresponding binding energies of the most stable $Pd_{1–6}/C_{10}H_6$ clusters obtained by the DFT method. The Mulliken orbital occupations of the single adsorbed Pd atom ($4s^{1.98}4p^{5.99}4d^{7.49}5s^{0.36}5p^{0.14}5d^{1.62}6s^{0.27}6p^{0.002}$) confirm extremely high AC-induced excitation in the palladium electronic structure with large deficit in the *d* electron density and significant occupation of the diffusive *s* and *p* orbitals. That results in close similarity in the shape of the $Pd_n/C_{10}H_6$ and $Pd_n/AC_{1,H}$ clusters obtained by the two methods. However, incorporation of the diffusive orbitals into DFT calculations causes destabilization of the planar conformers growing in the plane of aromatic rings (structures *3–6d*/$AC_{1,H}$ in Fig. 4) and promotes elongation of Pd–C and Pd–Pd bonds with simultaneous increase of the adsorption energies. Moreover, full optimization of the Pd_n and $C_{10}H_6$ geometries performed in the DFT calculations in comparison with the symmetry-constrained optimization of the metal clusters and frozen geometry of the support model applied in the EH calculations also contribute to the differences in the absolute energy values. Small size of the $C_{10}H_6$ cluster modeling the support surface results in some overestimation of the Pd–AC binding energy obtained by the DFT method (∼3–5 kcal/mol, as shown the EH energy differences between Pd_n adsorption on the $AC_{1,H}$ and $C_{10}H_6$ clusters) and overrates the adsorbent-induced relaxation of the support.

Our comparison confirms again that electronic structures from EH calculations are very consistent with those from high-level methods. In contrast, EH methods are known to provide poor absolute values of bond lengths and energies. Thus, the EH optimized Pd–Pd and Pd–C bond lengths are underestimated in comparison with the corresponding DFT values. As in the case of bare palladium clusters and ions, in the Pd_n/AC systems the EH and DFT binding energies differ significantly, while qualitatively the size dependences are similar. The EH binding energies in the Pd_n/AC ($n = 2$–6) system show the linear dependence on the corresponding DFT values similar to that presented in Fig. 1:

$$E_{EH} = 0.19E_{DFT} + 66.32 \quad \left(R^2 = 0.99\right). \tag{3}$$

The former coefficient here represents mainly the DFT correction to the Pd–Pd binding energy whereas the latter one is generally responsible for the interaction of the first-layer palladium atoms with the support and with each other. Therefore, at the qualitative level, the EH method provides agreement with the DFT results reasonable enough for its application for larger systems.

4.2. Directions for further cluster growth

Two energetically favorable directions for further growth of the most stable Pd_6 isomer (*6c*/$AC_{1,H}$ in Fig. 4) are shown in Fig. 6a. The first one starts with incorporation of two additional palladium atoms into the bottom layer. The resulting structure presents the most stable Pd_8 isomer, which further grows into the relatively stable *9b–15b*/$AC_{1,H}$ conformers. However, starting from nine-atomic clusters, formation of the close-packed upper-layer arrangement very similar to the curved *fcc* (111) face (*9c*/$AC_{1,H}$) becomes energetically more favorable. The structures *11c–16a*/$AC_{1,H}$ present the preferential way for the growth of Pd particles on the two-center position of the AC surface.

$Pd_{8–15}$ clusters growing in these two ways show many common features. All these clusters have a compact bulk structure with average Pd–Pd bond occupations far from the AC surface of 0.07–0.10, i.e., slightly higher than those in the bulk. With increasing coordination saturation of surface palladium atoms, their interaction with each other becomes close to that on the low-index bulk surfaces (see Table 2).

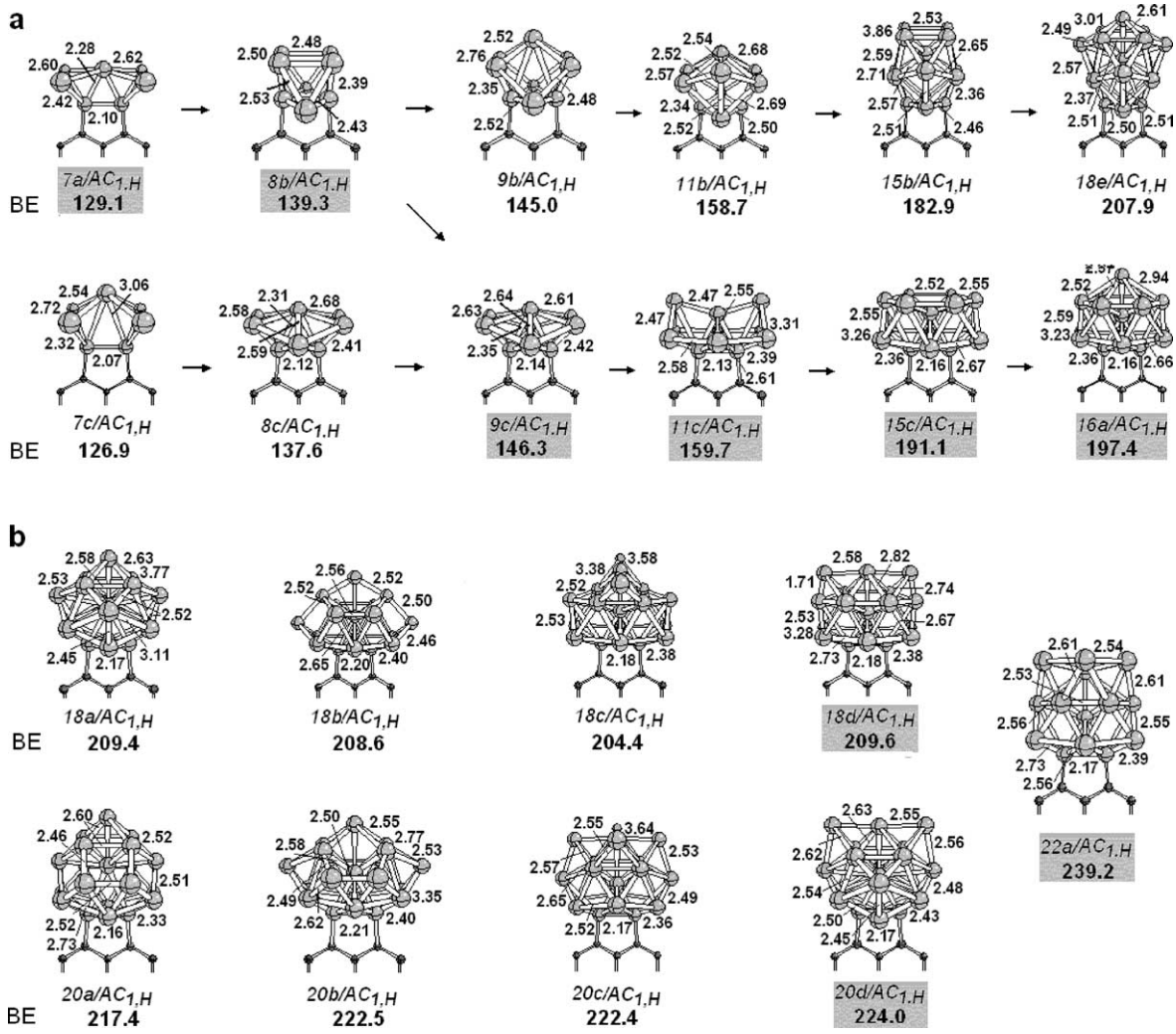

Fig. 6. The most likely directions for the growth of palladium particles in the two-center coordination position of the saturated regular zigzag edge modeled by the $AC_{1,H}$ cluster.

The lowest layer Pd atoms form much stronger bonds. The surfaces of the clusters are close-packed with preferentially triangular arrangement of metal atoms. Formation of more "open" surface assemblies is energetically unfavorable. Finally, structural differences extend only to the lowest layers. Geometric and electronic configurations of surface layers of the $18e/AC_{1,H}$ and $16a/AC_{1,H}$ clusters are very similar. Both these clusters could serve as nucleation centers of bulk *fcc* structure.

In Fig. 6b, several possibilities for incorporation of additional two and four palladium atoms into the *16a* cluster are considered. Comparing the energetics of the *18a*–*18d*$/AC_{1,H}$ structures, one can see that the additional atoms continue to build the upper layer started by the topmost Pd atom in the $16a/AC_{1,H}$ structure with preferential direction in the plane of $AC_{1,H}$ cluster. The inclusion of two Pd atoms into each of the two upper layers presents the most stable configuration of the supported $Pd_{20}/AC_{1,H}$ cluster. Finally, structure $22a/AC_{1,H}$ shows the most stable 22-atomic cluster with an average diameter of 13 Å. Summarizing the above results, we suppose that minimization of the surface energy presents the main factor determining growth of nanosized clusters.

Increasing cluster size leads to a slight decrease of the electron density on palladium atoms directly bound to carbon. Most likely, essential positive charge on these atoms induces the high Pd_{3d} binding energies in the Pd/AC clusters of a mean diameter less than 1 nm observed experimentally [63]. The electronic structure of the surface Pd atoms shows only minor dependence on the cluster size. These atoms have the electronic configuration $4d^{9.7–9.8}5s^{0.1–0.2}5p^{0.1}$ and maintain small (~ 0.05–0.1) negative charge, which arises from slightly higher occupations of Pd $5s, p$ orbitals as compared to those on the bulk surfaces. This excess of electron density is due to the back-donation from the AC surface that allows for compensation of high positive charge on the first-layer palladium atoms and determines total negligible charging effects in the Pd_n–AC interaction observed experimentally [64].

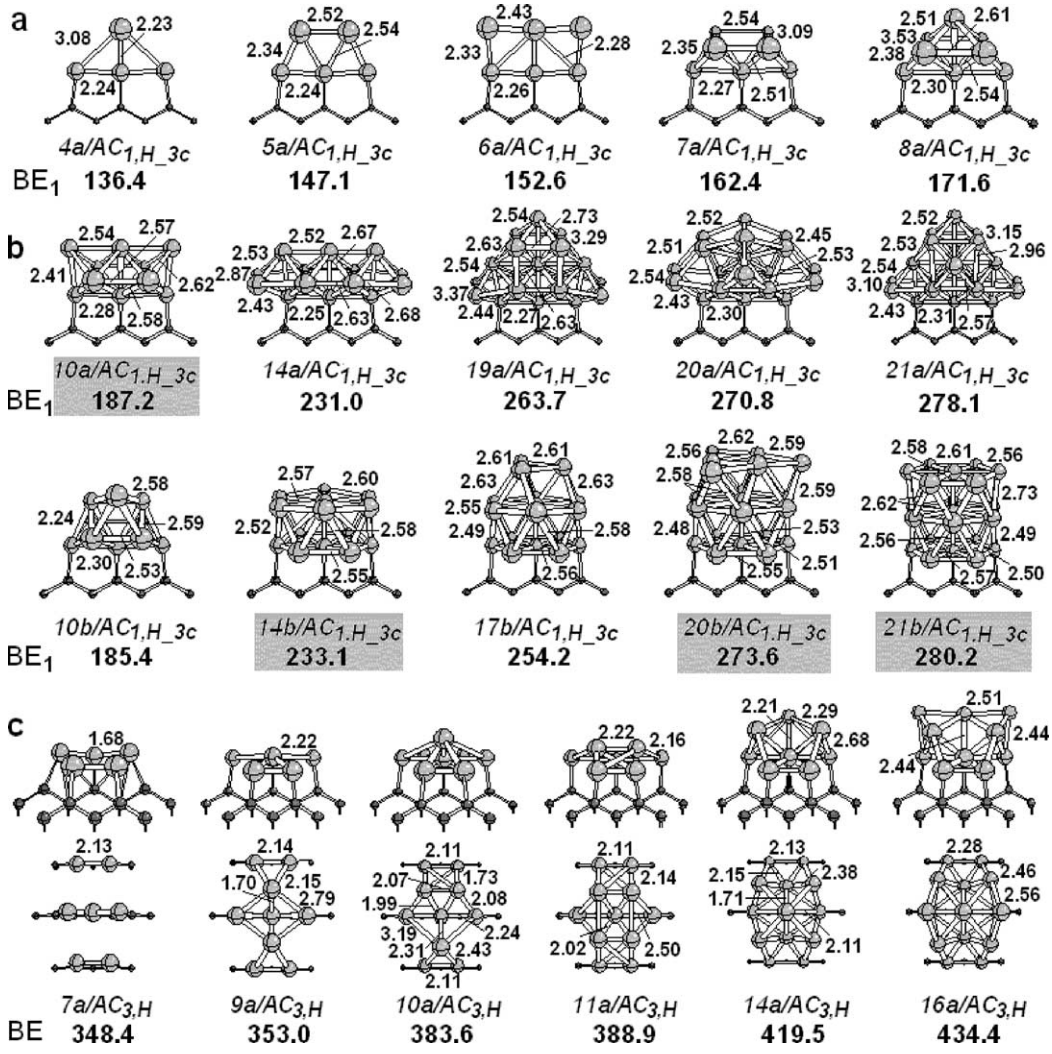

Fig. 7. Small palladium clusters adsorbed in the three-center coordination position of the saturated regular zigzag edge modeled by the AC_{1,H_3c} cluster (a), two preferential directions for their further growth (b), and the favorable way for the growth of palladium particles on the three-layer model cluster $AC_{3,H}$ (c) (the lower line presents the top view).

4.3. Palladium clusters on three C atoms of the zigzag edge

Small supported Pd clusters adsorbed in the three-center site of the one-layer model cluster (Fig. 7a) behave very similar to those adsorbed on the two-center site. In the most stable ten-atomic cluster ($10a/AC_{1,H\_3c}$ in Fig. 7b), the third-layer atoms form much shorter and stronger bonds with the first- than with the second-layer atoms. Further growth of this cluster leads to the formation of the $14a/AC_{1,H\_3c}$–$21a/AC_{1,H\_3c}$ configurations with relatively high surface area. Therefore, starting from 14-atomic clusters, formation of the close-packed arrangements very similar to those discussed above (cp., e.g., structures $14b/AC_{1,H\_3c}$ in Fig. 7b and $15c/AC_{1,H}$ in Fig. 6a) becomes energetically more favorable. While two-layer $14b/AC_{1,H\_3c}$ and three-layer $21b/AC_{1,H\_3c}$ configurations are not consistent with the palladium bulk structure, the preferential direction for the cluster growth presented by the $17b/AC_{1,H\_3c}$ and $20b/AC_{1,H\_3c}$ clusters exhibits development of the *fcc* structure with triangular (111) faces.

4.4. Palladium clusters on the three-layer model cluster

On the three-layer model cluster, palladium atoms adsorbed on the sequential graphite layers optimize their interactions with the coordination sites and exhibit negligible interaction with each other ($7a/AC_{3,H}$ in Fig. 7c). The best position for the next four atoms is between metal atoms adsorbed on different layers ($9a$–$11a/AC_{3,H}$). These atoms form extremely strong bonds with the central Pd atom. However, further cluster growth ($14a/AC_{3,H}$) leads to the structural transformations in the first layer: the $9a/AC_{3,H}$ cluster provides the connection to the support, and other atoms are pushed into the upper layers. The geometric and electronic structures of the upper-layer atoms in the $16a/AC_{3,H}$ cluster are very similar to those of the $10a/AC_{1,H\_3c}$ cluster. Thus,

we suppose that further cluster growth will proceed in an analogous manner.

4.5. Palladium clusters on the model defect of the AC surface

The model defect site on the AC surface provides the strongest interactions with a single palladium atom and with palladium dimer and presents the most likely nucleation center. The likely direction for the growth of palladium clusters in this adsorption position is shown in Fig. 8a. The first four atoms are directly bound to the support. Further cluster growth faces the steric restrictions due to the nearest neighboring hydrogen atoms. For that reason, up to 10-atomic clusters grow outward from the support surface and hold "open" surfaces with low-coordinated metal atoms. Starting from $11a/AC_{d,H}$, the development in the plane of aromatic rings becomes possible and the clusters form again close-packed triangular surfaces. The geometric and electronic structures of the upper-layer metal atoms in the $13a/AC_{d,H}$ cluster are very close to those in the similar clusters adsorbed on the regular zigzag edges.

Figure 8b presents the most stable configurations of small palladium clusters growing on the same model defect site with two hydrogen atoms in the nearest neighboring to the defect site positions being removed. In general, the cluster growth follows the regularities described above and for the $13a/AC_{d,H\_3c}$ cluster the geometric structure of the upper layer is similar to the curved *fcc* (111) plane. However, due to the higher unsaturation of the AC_{d,H_3c} coordination site, the interatomic Pd–Pd distances are significantly contracted as compared to those in palladium clusters on the regular zigzag edges.

Summarizing, the geometry of few-atomic clusters strongly depends on the morphology of the particular AC adsorption site while larger clusters form bulk *fcc*-like structures with nearly spherical shape and close-packed triangular surfaces. Electronic structure of very small supported particles varies significantly with structure and chemical nature of the adsorption position but remains about the same for the outer atoms in relatively large three-layer clusters.

5. Discussion

Obtained results have some implications to the understanding of the Pd–AC interaction and its effect on the catalytic reactivity of supported metal catalysts. In this section, we link the computational data and the experimental observations.

5.1. Atomic phase Pd/AC catalysts

Carbon supports consist generally from small graphite crystallites. That results in high surface area presented by basal graphite planes and numerous grain boundaries and dislocations containing unsaturated carbon atoms and functional groups. Our calculations show that the basal graphite plane is inactive toward palladium adsorption. In contrast, Pd_n/AC particles are strongly bound to various unsaturated surface sites. For this reason, HOPG and other graphite materials, which are usually used as carbon model supports [10,65], seem to not be representative of transition metal/AC catalysts.

From the adsorption sites on the most common regular zigzag edges of AC grains, the twofold position between nearest aromatic rings (labeled *d* in Fig. 3) is energetically the most favorable at very low loading. In these positions, supported metal atoms tend to be situated as far from each other as possible and are easily available for catalytic interactions. Adsorption in this position provides the best interaction between Pd 4*d* orbitals and the aromatic π system and results in the strong excitation in the palladium electronic structure with notable occupation of the 5*s* AO and large deficit in the 4*d* electron density. That, in turn, should cause the specific chemical and physical properties of highly dispersed Pd/AC catalysts. With increasing concentration of supported palladium atoms, stability of the twofold positions decreases, and the metal atoms shift to the onefold *e* positions. Filling of the onefold surface sites on the regular zigzag edges takes place up to the monolayer coverage. In such positions, adsorbed palladium atoms acquire high 5*s* AO occupation while excitations in the 4*d* electron density are less pronounced than in the twofold sites. Further increase of Pd loading leads to nucleation of supported clusters.

Surface defects are especially active toward capping of palladium atoms with the stability of each particular surface site being strongly dependent on its geometric structure and chemical nature. Strong bonding of adsorbed palladium atoms to defect sites, where several Pd–C bonds could form, confirms the suggestion of authors [44] about deposition of metal particles of high dispersion in narrow pores of the supports, which can render part of the metal surface inaccessible to reactants of catalytic reaction. Highly stable adsorption positions at boundaries of micro- and nanopores present the most likely nucleation centers, on which supported palladium particles grow. Probably, it causes notable decrease of AC surface area at impregnation [66].

Interaction of palladium atoms with various unsaturated and defect sites on the AC surface is much stronger than that with each other. Consequently, while Pd_n–AC binding energy tends to increase with increasing cluster size, the adsorption energy per palladium atom decreases systematically. That provides the driving force for rising dispersity of Pd/AC catalysts at elevated reduction temperatures observed experimentally [44,45,67]. In contrast, at relatively low temperatures, the high activation barrier for surface diffusion of a palladium atom favors the preservation of spatial adsorbed particles formed at the calcination step. On the other hand, highly activated diffusion and strong bonding of adsorbed particles to the support make their sintering ener-

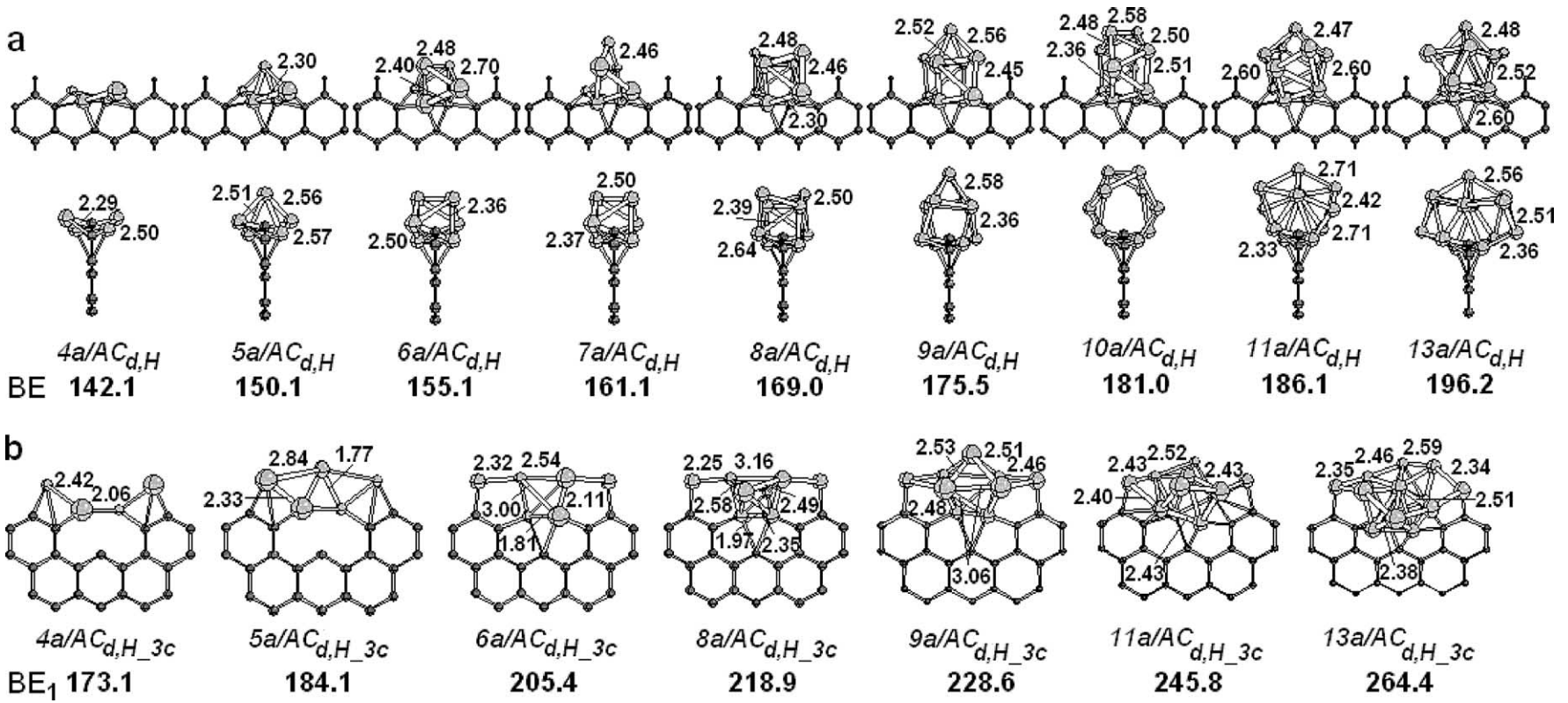

Fig. 8. Optimized structures and corresponding binding energies (kcal/mol) of Pd_n/AC ($n = 4$–13) clusters bound to the defect site on the $AC_{d,H}$ and AC_{d,H_3c} model clusters (the lower line in Fig. 8a presents the side view).

getically unfavorable. We suppose that the experimentally observed decrease in the Pd/AC dispersity at the reduction temperature higher than 400 K [44] is due to palladium-catalyzed alterations in the support surface structure rather than to the diffusion-controlled agglomeration. This issue will be discussed in a future communication of ours. Thus, in agreement with the experimental observations [44], from the thermodynamic point of view, the atomic palladium dispersion could be achieved at the proper reduction conditions. Taking into account high surface area of common activated carbon supports, one can expect that in real Pd/AC catalysts a significant part of metal particles exists in the atomically dispersed form.

Similar effects could underly the anomalous nucleation of Pd, Ni, and Ag particles on amorphous carbon observed in the vapor deposition experiments [2]. Trapping of metal atoms at the most stable sites does not lead to the clusters nucleation until the monolayer saturation is achieved. Further deposition of metal atoms causes their rapid coalescence.

5.2. Functional groups on the AC surface

Activated carbons derived from different sources or subjected to various pretreatment procedures are characterized by different porous structure and surface composition. Our consideration is restricted to the second subject. Saturation of dangling surface bonds causes destabilization of adsorption positions on the regular zigzag edges but the nature of surface groups (H or OH) has only a minor effect. The saturation of dangling surface bonds is expected to decrease the dispersity of supported palladium particles by means of a decreasing number of active sites on the AC surface and limitation of their surface motion. Moreover, on saturated surfaces a much larger fraction of supported particles is expected to occupy out-of-the-way places in nanopores than that on unsaturated surfaces. Experimentally, this effect manifests itself in the profound influence of the origin of carbon support on the properties of the palladium catalysts and in the absence of unambiguous correlation between catalyst properties and pretreatment of activated carbons [45]. Owing to the long-range charge transfer along the aromatic π system, palladium adsorption causes notable alterations in surface bonds of the support, which significantly contribute to the apparent adsorption energy.

5.3. Supported Pd_n/AC clusters

Bulk and especially surface structure of supported transition metal particles is extremely important for their catalytic performance. At present, interpreting experimental data, the authors usually use models derived from the corresponding metal crystal structures and widely discuss crystal facets, kinks, and steps on cluster surfaces [2,8–10,12,13]. On the other hand, it is believed that interaction with a support causes remarkable changes in the electronic structure of supported metal particles. To the best of our knowledge, in the present work we make the first attempt to address this question from the theoretical point of view.

Our results show that the geometry of very small palladium clusters supported on the AC surface is determined by the structure of a particular adsorption site. However, further cluster growth always leads to the formation of compact particles with nearly spherical shape and close-packed triangular surface structure. More "open" surfaces are energetically unfavorable. In contrast to the bare palladium clusters, showing the tendency to form icosahedral configurations, activated carbon support enhances direct nucleation of the *fcc* bulk structure. For relatively small clusters ($n < 10$), the binding energy per palladium atoms sharply drops with increasing cluster size. That provides the driving force for high dispersity of adsorbed palladium on AC surface. For larger clusters, the binding energy per Pd atom becomes less sensitive to the cluster size; therefore, at favorable steric conditions large palladium particles could grow and coexist with relatively small supported clusters, as was observed experimentally [67]. Firm interaction between activated carbon and palladium particles and support-induced strengthening of the Pd–Pd bonding underly such an important technological characteristic as stability of the supported catalysts. These results are very consistent with the intuitive representation of the morphology of supported cluster; however, as will be seen from our future communications, this is not always in case.

Size dependencies of the binding energies for Pd_n adsorptions on the considered AC surface sites are well approximated by the linear relationship $BE = a*n + b$ (Fig. 9a). For the similar coordination positions (regular zigzag edge or defect site), the regression slope a increases with increasing surface unsaturation. The intercept b increases with strengthening the interaction between the first-layer Pd atoms and the support. With the adopted expressions for the calculation of BE and BE_1 (Eqs. (1) and (2)), it means that palladium displacement of hydrogen atoms in the nearest neighboring to the coordination site positions is energetically favorable and the energy gain of such substitution increases with increasing size of Pd_n cluster. Taking into account the excess of hydrogen, high temperature, and possible catalytic effect of adsorbed palladium particles, one can expect that palladium substitution of surface hydrogen readily proceeds in real systems. Fig. 9b demonstrates that the average Pd_n–AC interaction energy could be well approximated by the linear dependence on the number of Pd–C bonds formed, which in turn depends on the number of coordination positions available for Pd adsorption on AC surface. The linear relationships presented in Figs. 9a and 9b allow one to estimate the Pd_n–AC interaction energy for the given coordination position and cluster size. Using Eq. (3), one can estimate the DFT interaction energy for Pd_n adsorption on the regular zigzag edge of the AC surface. Unfortunately, we cannot estimate the relationship between EH and DFT energies for other coordination sites due to the computational difficulties.

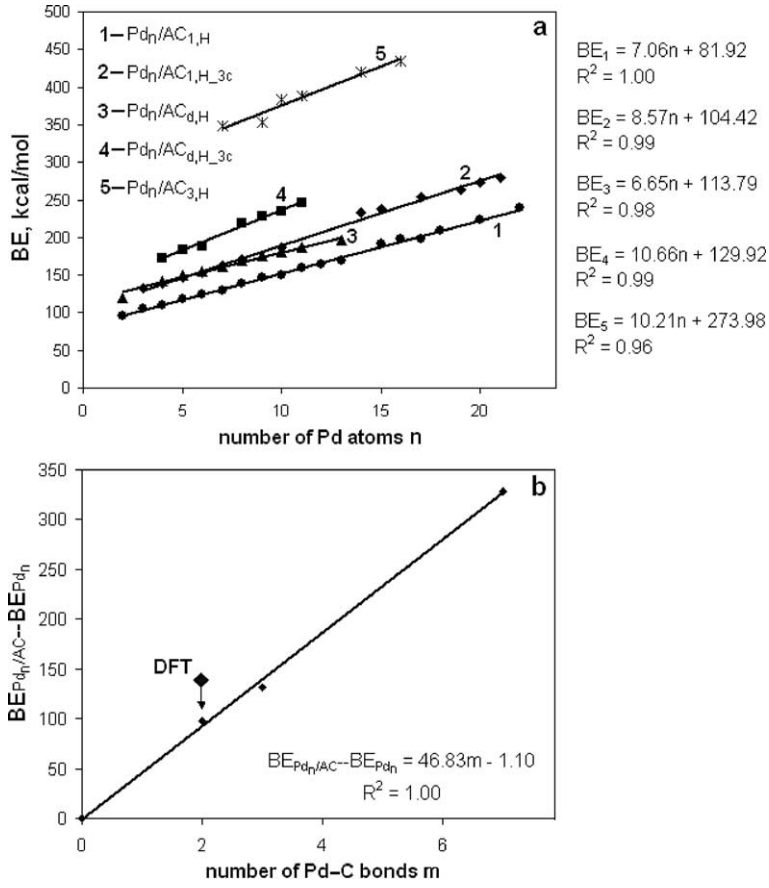

Fig. 9. Size dependence of the binding energy for Pd_n adsorption in different coordination positions on the AC surface (a) and Pd_n–AC interaction energy as a function of the number of occupied surface sites (b).

Although metals are characterized by easy charge transfer, we found that Pd–AC interaction has a very local nature with respect to supported particles and is strongly delocalized along the aromatic π system. Consequently, while electronic structure of the palladium atoms directly bound to the support surface is extremely excited, these alterations sharply diminish with height above the support. The electronic configuration of the upper-layer palladium atoms is very close to that of bulk surfaces with only slightly high 5*s* orbital occupations. Hence, in contrast to the atomic-phase Pd/AC, supported nanosized particles should exhibit chemical behavior very similar to that of the bulk.

Therefore, growth of AC-supported palladium particles at the catalyst reduction stage could be seen as follows. Palladium deposition starts from the filling of unsaturated surface positions up to the monolayer coverage followed by the formation of few-atomic clusters with geometry determined by the morphology and chemical nature of the adsorption site. Such clusters are located preferentially in defect sites and nanopores with high concentration of unsaturated carbon atoms. Electronic structure of Pd atoms in such clusters is extremely excited. These clusters grow into compact three-dimensional particles of about 1 nm in diameter. Surface atoms in such particles form close-packed triangular arrangements and have electronic configuration very similar to that of bulk. These particles serve as nucleation centers for the bulk *fcc* structure. Structure $16a/AC_{1,H}$ in Fig. 6a presents such simplest nucleus. Construction of each next layer begins from the deposition of Pd atoms above the upper-layer *fcc* sites followed by filling threefold positions at the cluster sides and is completed by Pd substitution of the nearest neighboring H atoms on the AC surface with formation of new Pd–C bonds. Supported particles growing by such a mechanism will have close to semispherical shape with minimal surface energy and effective Pd_n–AC interaction.

6. Conclusions

Geometric and electronic structures of palladium catalysts supported on activated carbon (AC) are analyzed using semiempirical quantum chemical modeling in comparison with DFT calculations and with published experimental data. The issues raised in the Introduction could be summarized as follows:

1. In contrast to the basal graphite plane, unsaturated surface carbon atoms are found to form very strong bonds with Pd atoms. The experimentally observed preferen-

tial palladium adsorption in narrow pores is attributed to a high concentration of unsaturated surface bonds in these adsorption positions. At very low loading, palladium atoms on AC surface are positively charged due to the extremely effective delocalized donor–acceptor interaction with the π system of the support. Increasing loading causes alterations in the Pd–AC bonding accompanied by diminishing deficit in Pd 4*d* electron density and corresponding net charge.

2. Pretreatment of the AC surface decreases the number of surface sites available for adsorption of metal particles and causes pronounced stabilization of adsorption positions in micro- and nanopores as against coordination sites on zigzag edges of AC grain boundaries. Saturation of dangling surface bonds significantly contributed to the energetics of Pd–AC interactions. The nature of surface groups has only a minor influence on the Pd–AC bonding.
3. Interactions of Pd atoms with AC surface sites are by far stronger than with each other. That provides the driving force for atomic dispersity of Pd/AC catalysts. Together with a high activation barrier for Pd surface diffusion, that manifests itself experimentally in increasing Pd dispersion with increasing catalyst reduction temperature. Cluster formation becomes thermodynamically preferential after the saturation of monolayer coverage. Taking into account high surface area of the usual AC supports, we suppose that a large part of supported palladium exists in the atomically dispersed form.
4. Geometry of very small supported clusters essentially depends on the morphology of a particular coordination site. As opposed to the gas-phase clusters, the support-induced changes in the Pd electronic structure result in the direct nucleation of the *fcc* structure. With increasing cluster size, the Pd_n–AC bonding strengthens.
5. Further cluster growth leads to the formation of compact three-dimensional particles with close-packed preferentially triangular surfaces. While electronic structure of the palladium atoms directly bound to the support is extremely excited, these alterations sharply diminish with height above the support so that the electronic configuration of the surface atoms in nanosized palladium clusters is very close to that of the low-index bulk surfaces. For that reason, we speculate that nanosized palladium particles supported on the AC surface behave very similar to the close-packed bulk palladium surfaces.

Acknowledgments

This research was supported by the Ministry of Science. I.E. is partially supported by the Center for Absorption in Science, State of Israel. M.S. is a member of the Institute of Catalysis of the Technion.

References

[1] S.P. Gubin, Chemistry of Clusters: Fundamentals of Classification and Structure, Nauka, Moscow, 1987 (In Russian).
[2] R. Anton, A.A. Schmidt, Surf. Sci. 357–358 (1996) 835.
[3] A.W. Castleman Jr., K.H. Bowen Jr., J. Phys. Chem. 100 (1996) 12911.
[4] P. Fayet, A. Kaldor, D.M. Cox, J. Chem. Phys. 92 (1990) 254.
[5] M. Che, C.O. Bennett, Adv. Catal. 36 (1989) 55.
[6] W. Eberhardt, Surf. Sci. 500 (2002) 242.
[7] Y. Volokitin, J. Sinzig, L.J. de Jongh, G. Schmid, M.N. Vargaftik, I.I. Moiseev, Nature 384 (1996) 621.
[8] F. Zaera, Prog. Surf. Sci. 69 (2001) 1.
[9] C.R. Henry, Appl. Surf. Sci. 164 (2000) 252.
[10] P.L.J. Gunter, J.W. Niemantsverdrit, F.H. Ribeiro, G.A. Somorjai, Catal. Rev.-Sci. Eng. 39 (1997) 77.
[11] H. Poppa, Catal. Rev.-Sci. Eng. 35 (1993) 359.
[12] H.-J. Freund, M. Bäumer, H. Kuhlenbeck, Adv. Catal. 45 (2000) 333.
[13] C. Binns, Surf. Sci. Rep. 44 (2001) 1.
[14] C.T. Campbell, A.W. Grant, D.E. Starr, S.C. Parker, V.A. Bondzie, Top. Catal. 14 (2001) 43.
[15] R.M. Lambert, G. Pacchioni (Eds.), Chemisorption and reactivity on supported clusters and thin films, towards an understanding of microscopic processes in catalysis, in: Proceedings of the NATO Advanced Study Institute, Erice, Trapani, Sicily (July 15–26, 1996), Kluwer, Dordrecht, 1997.
[16] K.M. Neyman, G. Pacchioni, N. Rosch, Theor. Comput. Chem. 4 (1996) 569.
[17] S. Abbet, U. Heiz, A.M. Ferrari, L. Giordano, C. Di Valentin, G. Pacchioni, Thin Solid Films 400 (2001) 37.
[18] L. Giordano, J. Goniakowski, G. Pacchioni, Phys. Rev. B 64 (2001) 075417/1.
[19] S. Abbet, E. Riedo, H. Brune, U. Heiz, A.M. Ferrari, L. Giordano, G. Pacchioni, J. Am. Chem. Soc. 123 (2001) 6172.
[20] K.M. Neyman, N. Rosch, G. Pacchioni, Appl. Catal. A 191 (2000) 3.
[21] A.M. Ferrari, C. Xiao, K.M. Neyman, G. Pacchioni, N. Rosch, Phys. Chem. Chem. Phys. 1 (1999) 4655.
[22] A.V. Matveev, K.M. Neyman, G. Pacchioni, N. Rosch, Chem. Phys. Lett. 299 (1999) 603.
[23] K.M. Neyman, S. Vent, G. Pacchioni, N. Rosch, Nuovo Cimento Soc. Ital. Fis. D 19 (1997) 1743.
[24] I.V. Yudanov, S. Vent, K. Neyman, G. Pacchioni, N. Roesch, Chem. Phys. Lett. 275 (1997) 245.
[25] A.M. Ferrari, G. Pacchioni, J. Phys. Chem. 100 (1996) 9032.
[26] N. Lopez, F. Illas, J. Phys. Chem. B 102 (1998) 1430.
[27] L. Giordano, G. Pacchioni, T. Bredow, J.F. Sanz, Surf. Sci. 471 (2001) 21.
[28] G. Pacchioni, N. Roesch, J. Chem. Phys. 104 (1996) 7329.
[29] A. Markovits, M.K. Skalli, C. Minot, G. Pacchioni, N. Lopez, F. Illas, J. Chem. Phys. 115 (2001) 8172.
[30] L. Giordano, G. Pacchioni, A.M. Ferrari, F. Illas, N. Rosch, Surf. Sci. 473 (2001) 213.
[31] N. Lopez, F. Illas, G. Pacchioni, J. Am. Chem. Soc. 121 (1999) 813.
[32] N. Lopez, F. Illas, G. Pacchioni, J. Mol. Catal. A 170 (2001) 175.
[33] G. Pacchioni, N. Lopez, F. Illas, Faraday Discuss. 114 (1999) 209.
[34] N. Lopez, F. Illas, G. Pacchioni, J. Phys. Chem. B 103 (1999) 1712.
[35] J.R.B. Gomes, F. Illas, N.C. Hernandez, J.F. Sanz, A. Wander, N.M. Harrison, J. Chem. Phys. 116 (2002) 1684.
[36] G. Pacchioni, N. Roesch, Surf. Sci. 306 (1994) 169.
[37] G.R. Hennig, Chem. Phys. Carbon 2 (1966) 1.
[38] H.P. Boehm, Adv. Catal. 16 (1966) 179.
[39] P. Pfeifer, F. Ehrburger-Dolle, T.P. Rieker, M.T. González, W.P. Hoffman, M. Molina-Sabio, F. Rodríguez-Reinoso, P.W. Schmidt, D.J. Voss, Phys. Rev. Lett. 88 (2002), article 115502/1.
[40] M. Voll, H.P. Boehm, Carbon 9 (1971) 473.
[41] M. Voll, H.P. Boehm, Carbon 8 (1970) 741.
[42] H.P. Boehm, Carbon 40 (2002) 145.

[43] H.P. Boehm, Carbon 32 (1994) 759.
[44] L.B. Okhlopkova, A.S. Lisitsyn, V.A. Likholobov, M. Gurrath, H.P. Boehm, Appl. Catal. A 204 (2000) 229.
[45] M. Gurrath, T. Kuretzky, H.P. Boehm, L.B. Okhlopkova, A.S. Lisitsyn, V.A. Likholobov, Carbon 38 (2000) 1241.
[46] A. Juan, R. Hoffmann, Surf. Sci. 421 (1999) 1.
[47] W.V. Glassey, R. Hoffmann, J. Phys. Chem. B 105 (2001) 3245;
W.V. Glassey, R. Hoffmann, Surf. Sci. 475 (2001) 47;
P. Hermann, D. Simon, P. Sautet, B. Bigot, J. Catal. 167 (1997) 33;
F. Delbecq, P. Sautet, J. Catal. 164 (1996) 152;
F. Delbecq, P. Sautet, J. Catal. 152 (1995) 217.
[48] I. Efremenko, M. Sheintuch, Surf. Sci. 414 (1998) 148.
[49] I. Efremenko, M. Sheintuch, J. Mol. Catal. A 160 (2000) 445.
[50] R. Stowasser, R. Hoffmann, J. Am. Chem. Soc. 121 (1999) 3414.
[51] C. Xiao, S. Kruger, T. Belling, M. Mayer, N. Rosch, Int. J. Quantum Chem. 74 (1999) 405.
[52] R. Hoffmann, W.N. Lipscomb, J. Chem. Phys. 36 (1962) 2179;
R. Hoffmann, W.N. Lipscomb, J. Chem. Phys. 37 (1962) 2872;
R. Hoffmann, J. Chem. Phys. 39 (1963) 1397.
[53] A.B. Anderson, J. Chem. Phys. 62 (1975) 1187;
A.B. Anderson, R.W. Grimes, S.Y. Hong, J. Phys. Chem. 91 (1987) 4245.
[54] J.H. Ammeter, H.-B. Bürdi, J.C. Thibeault, R. Hoffmann, J. Am. Chem. Soc. 100 (1978) 3686.
[55] K. Tatsumi, R. Hoffmann, A. Yamamoto, J.K. Stille, Bull. Chem. Soc. Jpn. 54 (1981) 1857.
[56] G. Calzaferri, L. Forss, I. Kamber, J. Phys. Chem. 93 (1989) 5366;
F. Savary, J. Weber, G. Calzaferri, J. Phys. Chem. 97 (1993) 3722.
[57] M.J. Frisch, G.W. Trucks, H.B. Schlegel, G.E. Scuseria, M.A. Robb, J.R. Cheeseman, V.G. Zakrzewski, J.A. Montgomery Jr., R.E. Stratmann, J.C. Burant, S. Dapprich, J.M. Millam, A.D. Daniels, K.N. Kudin, M.C. Strain, O. Farkas, J. Tomasi, V. Barone, M. Cossi, R. Cammi, B. Mennucci, C. Pomelli, C. Adamo, S. Clifford, J. Ochterski, G.A. Petersson, P.Y. Ayala, Q. Cui, K. Morokuma, D.K. Malick, A.D. Rabuck, K. Raghavachari, J.B. Foresman, J. Cioslowski, J.V. Ortiz, A.G. Baboul, B.B. Stefanov, G. Liu, A. Liashenko, P. Piskorz, I. Komaromi, R. Gomperts, R.L. Martin, D.J. Fox, T. Keith, M.A. Al-Laham, C.Y. Peng, A. Nanayakkara, C. Gonzalez, M. Challacombe, P.M.W. Gill, B. Johnson, W. Chen, M.W. Wong, J.L. Andres, C. Gonzalez, M. Head-Gordon, E.S. Replogle, J.A. Pople, Gaussian 98, Revision A.7, Gaussian, Inc., Pittsburgh, PA, 1998.
[58] A.D. Becke, J. Chem. Phys. 98 (1993) 5648.
[59] C. Lee, W. Yang, R.G. Parr, Phys. Rev. B 37 (1988) 785.
[60] P.J. Hay, W.R. Wadt, J. Chem. Phys. 82 (1985) 299.
[61] T.H. Dunning Jr., P.J. Hay, in: H.F. Schaefer III (Ed.), Methods of Electronic Structure, Theory, Vol. 2, Plenum Press, 1977.
[62] D.E. Woon, T.H. Dunning Jr., J. Chem. Phys. 98 (1993) 1358.
[63] H.N. Aiyer, V. Vijayakrishnan, G.N. Subbanna, C.N.R. Rao, Surf. Sci. 313 (1994) 392.
[64] M. De Crescenzi, F. Patella, N. Motta, M. Sastry, F. Rochet, R. Pasquali, A. Balzarotti, Solid State Commun. 73 (1990) 251.
[65] A. Piednoir, E. Perrot, S. Granjeaud, A. Humbert, C. Chapon, C.R. Henry, Surf. Sci. 391 (1997) 19.
[66] Yu. Shindler, Yu. Matatov-Meytal, M. Sheintuch, Ind. Eng. Chem. Res. 40 (2001) 3301.
[67] A. Benedetti, L. Bertoldo, P. Canton, G. Georigk, F. Pinna, P. Riello, S. Polizzi, Catal. Today 49 (1999) 485.